

OPEN ACCESS

Electrochemical Impedance Spectroscopy of Oxygen Reduction Reaction (ORR) in a Rotating Disk Electrode Configuration: Effect of Ionomer Content and Carbon-Support

To cite this article: Ramesh Kumar Singh *et al* 2015 *J. Electrochem. Soc.* **162** F489

View the [article online](#) for updates and enhancements.

You may also like

- [Spike sorting in the presence of stimulation artifacts: a dynamical control systems approach](#)
Mohammad Shokri, Alex R Gogliettino, Pawe Hottowy *et al.*
- [Nonequilibrium Ionization Effects on Coronal Plasma Diagnostics and Elemental Abundance Measurements](#)
Tong Shi, Enrico Landi and Ward Manchester
- [Embedded electrical impedance-based PZT sensor for monitoring hydrating concrete: development and evaluation](#)
Amarteja Kocherla and Kolluru V L Subramaniam



Your Lab in a Box!

The PAT-Tester-i-16: All you need for Battery Material Testing.

- ✓ All-in-One Solution with integrated Temperature Chamber!
- ✓ Cableless Connection for Battery Test Cells!
- ✓ Fully featured Multichannel Potentiostat / Galvanostat / EIS!

www.el-cell.com +49 40 79012-734 sales@el-cell.com

EL-CELL[®]
electrochemical test equipment





Electrochemical Impedance Spectroscopy of Oxygen Reduction Reaction (ORR) in a Rotating Disk Electrode Configuration: Effect of Ionomer Content and Carbon-Support

Ramesh Kumar Singh, Ruttala Devivaraprasad, Tathagata Kar, Arup Chakraborty, and Manoj Neergat^{*,z}

Department of Energy Science and Engineering, Indian Institute of Technology Bombay (IITB), Powai, Mumbai 400076, India

Oxygen reduction reaction (ORR) in acidic media is investigated at various potentials in a thin-film rotating disk electrode (TF-RDE) configuration using electrochemical impedance spectroscopy (EIS). The ionomer-free and ionomer-containing thin-film catalyst layers are composed of Pt black and carbon-supported Pt catalysts of different metal loadings (5 and 20 wt%). The simplest EIS spectrum consisting of an arc or a semi-circle is observed at high potentials with ionomer-free Pt catalyst layers. The most complex spectrum consisting of a high frequency (HF) arc and two semi-circles is observed in the mixed diffusion-controlled region of the ionomer-containing catalyst layer with high loading of carbon-supported Pt. The nature of the EI spectrum is decided by the constituents of the thin-film catalyst layer and by the operating potential. The evolution of the EI spectra with ionomer and carbon contents is underlined. The effect of rotation rate (rpm) of the electrode on the impedance spectrum is also investigated. A series of equivalent circuits is required to completely describe the EI spectra of ORR. The kinetic parameters and the electrochemical surface area of the catalysts are derived from the impedance spectrum.

© The Author(s) 2015. Published by ECS. This is an open access article distributed under the terms of the Creative Commons Attribution Non-Commercial No Derivatives 4.0 License (CC BY-NC-ND, <http://creativecommons.org/licenses/by-nc-nd/4.0/>), which permits non-commercial reuse, distribution, and reproduction in any medium, provided the original work is not changed in any way and is properly cited. For permission for commercial reuse, please email: oa@electrochem.org. [DOI: 10.1149/2.0141506jes] All rights reserved.

Manuscript submitted August 4, 2014; revised manuscript received February 2, 2015. Published February 24, 2015.

Oxygen reduction reaction (ORR) is one of the most important reactions at the cathode side in low-temperature fuel cells (e.g., polymer electrolyte fuel cells (PEFCs) and direct methanol fuel cells (DMFCs)) and metal-air batteries.¹⁻¹⁴ Because of the sluggish ORR kinetics and the stability issues of the catalyst in the electrochemical environment, expensive precious metal catalysts are often used in these electrochemical devices to catalyze the ORR.¹⁵ Conventionally, the performance of the catalyst is evaluated in an operating fuel cell mode using the DC methods.¹⁶⁻¹⁸ The information gathered from a DC analysis usually provides the sum of various polarizations of the electrode, which is difficult to separate into individual contributions.¹⁹ On the other hand, electrochemical impedance spectroscopy (EIS), one of the AC methods, is a sensitive tool to investigate electrode-electrolyte interface and it allows the simultaneous resolution of various charge-transfer and mass-transfer processes (kinetic, ohmic, and diffusion). It involves a small sinusoidal electrical perturbation around a steady-state value and measures the impedance along with the phase angle. However, the interpretation of the EI spectra is difficult. Often, simple fitting models based on equivalent circuit analogues and physical models are used to extract the parameters those represent the underlying cell processes.²⁰⁻²⁶

Springer et al. proposed the theoretical impedance spectrum of ORR on porous gas-diffusion electrode using the flooded-agglomerate electrode model in series with a thin electrolyte film.^{20,25} The model predicted by Raistrick shows three semi-circles in the spectrum attributed to the charge-transfer process (ORR); agglomerate diffusion (depletion of the oxygen concentration in the pores of the diffusion layer); and thin-film diffusion (diffusion of oxygen through the thin electrolyte/ionomer film to the catalyst sites).²¹ Since then, EIS has been used to characterize ORR in the fuel cell configuration.²²⁻²⁸ Springer et al. later characterized PEFC cathode supplied with oxygen/air using EIS and reported the effect of mass-transfer and humidification.²⁵ Parthasarathy et al. reported diffusion coefficient of oxygen through a thin-film layer of Nafion and diffusion-layer thickness from the finite-length Warburg behavior using the EI spectra of ORR on platinum/Nafion interface in PEFC configuration.²⁹ Ciureanu et al. investigated the effect of operating temperature, air-flow rate, and humidification of H₂/air fuel cell cathode.²⁶ Recently,

Piela et al. investigated methanol oxidation reaction (MOR), the poisoning effect of CO at the anode side in DMFC, and the effect of methanol crossover on ORR using EIS.¹⁹ Antolini et al. reported the effect of ionomer and Teflon contents on the performance of gas diffusion electrodes.^{30,31} Recently, Holdcroft critically reviewed the role of ionomer in the catalyst layer on the performance of fuel cell electrodes.³² A review of the literature reveals that a wide variety of spectra is reported depending on the operating conditions. Moreover, the assignment of the spectral features to physical processes are not conclusive in the literature; for e.g., the low frequency (LF) loop is attributed to slow diffusion of oxygen through the backing,^{25,26} back diffusion of water in the membrane,³³ or diffusion of water in the catalyst layer.³⁴

Since fuel cell involves several interfaces, EIS studies have also been conducted in half-membrane electrode assembly (MEA) configuration^{35,36} and the ORR kinetics was validated based on the mechanism proposed by Damajanovic et al.^{37,38} To further simplify the spectra, Perez et al. investigated the ORR in acidic and alkaline media in a thin-film rotating disk electrode (TF-RDE) configuration; moreover, the kinetic parameters obtained from the AC method were correlated with those obtained from the DC method.³⁹⁻⁴¹ Otherwise, the EIS of ORR on Pt in a three-electrode RDE system is seldom reported in the literature. Most importantly, the EI spectra of ORR in RDE configuration are entirely different from those of the theoretical and experimental impedance spectra consisting of two or three semi-circles reported in literature on fuel cell cathode with porous gas-diffusion electrode.²⁵

In an attempt to improve the kinetics of ORR and to reduce the overall cost of fuel cells, several new catalyst formulations have been investigated. These include, in addition to Pt-based materials, chalcogenides, Pd alloys, and non-precious metal catalysts.^{4-6,42-47} TF-RDE/rotating ring disk electrodes (RRDE) are popular in the characterization of these new catalyst formulations. Usually, this is done in aqueous electrolytes (0.1 M KOH, 0.1 M HClO₄ or 0.5 M H₂SO₄) or non-aqueous electrolytes (lithium bis(trifluoromethyl)sulfonyl imide (LiTFSI) in diglyme) using DC methods.^{12,48-51} This method is convenient and cost-effective since minute quantity (micrograms) of the catalyst is enough for the characterization. Moreover, the single-electrode study with TF-RDE/RRDE is simple since the complications arising from the other components of the fuel cell system are eliminated; particularly, from the anode and membrane electrolyte. Kinetic

*Electrochemical Society Active Member.

^zE-mail: nmanoj@iitb.ac.in

parameters those decide the quality of the catalyst can be easily derived from such measurements.

In this study, the EIS characterization of the ORR in a three-electrode configuration is reported with ionomer-free and ionomer-containing thin-film catalyst layers consisting of unsupported and carbon-supported platinum of various metal loadings. The origin of the LF semi-circle is inferred from the dependence of EI spectra on the ionomer content in the thin-film catalyst layer. The strong dependence of the diameter of the LF semi-circle on the rotation rate (rpm) of the electrode further confirms that the process is affected by the mass-transfer limitations of oxygen from the bulk of the solution to the active catalyst sites. Our investigation helps in identifying the appropriate equivalent circuits depending on the constituents of the thin-film catalyst layer and potential. Thus, a series of equivalence circuits of increasing complexity is proposed to describe EIS of ORR in the RDE configuration. Through these systematic investigations, we are able to assign the EI spectra of ORR at different frequency regions to the appropriate physical processes. To the best of our knowledge, this is the first report that discusses the complete impedance spectra of ORR on catalyst layers of various compositions in TF-RDE configuration over the relevant potential range of fuel cell cathode.

Experimental

Materials.— Dihydrogenhexachloroplatinate (IV) hexahydrate ($\text{H}_2\text{PtCl}_6 \cdot 6\text{H}_2\text{O}$) and Nafion suspension (5 wt% solution in lower aliphatic alcohols/ H_2O) from Sigma Aldrich; Pt black (HiSPEC 1000) from Alfa Aesar; perchloric acid (HClO_4 , 70% GR), sulfuric acid (H_2SO_4 , 98% GR), sodium hydroxide (NaOH), and sodium borohydride (NaBH_4) from Merck; and hydrogen peroxide (H_2O_2 , 30% by weight) from Loba Chemie were used as-received without any further purification. High purity (18.2 M Ω) de-ionized (DI) water was obtained from Direct Q Millipore.

Catalyst synthesis and electrode preparation.— Carbon-supported Pt (5 and 20 wt% metal loading on Vulcan XC-72) was synthesized *via* low-temperature NaBH_4 reduction. The details of catalyst synthesis and electrode preparation are explained in the experimental section (S1) of the supporting information (SI).

Electrochemical characterization and impedance spectroscopy.— The impedance spectra were recorded in a three-electrode TF-RDE configuration. High area Pt coil (5 cm^2) was used as the counter electrode to avoid the capacitive losses; catalyst-coated glassy-carbon disk electrode (0.196 cm^2) was used as the working electrode; Ag/AgCl (saturated KCl) was used as the reference electrode. All the potentials are reported with reference to reversible hydrogen electrode (RHE). The rotation speed (rpm) of the electrode was controlled using a modulated speed rotator from Pine Instruments. The cyclic voltammograms (CVs), ORR voltammograms, and impedance spectra were recorded using a 'PARSTAT 2273' (Advanced Electrochemical System) potentiostat (from Princeton Applied Research).

Prior to impedance measurements, CVs were recorded in an argon-saturated 0.1 M HClO_4 solution. Thereafter, the ORR voltammograms were recorded in an oxygen-saturated 0.1 M HClO_4 solution at 1600 rpm. All the voltammograms (CVs and ORR) were recorded at a scan rate of 20 mV s^{-1} from 0.05 to 1.05 V at room temperature (25°C). The impedance spectra were recorded with an AC amplitude of 5 mV rms by sweeping the frequency from 10 kHz to ~ 0.02 Hz at 10 points per decade (data collection on logarithmic scale). All data were recorded in a single sine mode. The impedance spectra were fitted using complex non-linear least square (CNLS) method with "ZSimpWin" software from Solartron. To confirm the stability of the catalysts, the ORR voltammograms and CVs of all catalysts were recorded before and after the impedance measurements. Catalyst layers with low and high ionomer content refer to those prepared from the ink formulations with 8 and 40 μL of Nafion suspension, respectively

(see experimental section of the SI). Ionomer-free catalyst layer refers to that prepared from catalyst ink without Nafion suspension.

Results and Discussion

General patterns of the impedance spectra.— The impedance spectra of all the catalysts are recorded at three different regions of the ORR polarization curve: (i) kinetic region (> 850 mV); (ii) mixed diffusion-controlled region (~ 850 – 750 mV); and (iii) mass-transport region (< 750 mV). Depending on the potential and constituents of the catalysts layers, various equivalent circuit elements are used to model the underlying cell processes. The simplest spectrum, consisting of arc/semi-circle, is obtained in the kinetic region and it represents polarization resistance (R_p) across the electrode-electrolyte interface. In the equivalent circuit (EC), this arc/semi-circle is represented with an (R_p, Q_1) element, where, R_p is dominated by the charge-transfer resistance (R_1) at high potentials and by the mass-transfer resistance (R_2) at low potentials. Q_1 is the constant phase element (CPE₁) corresponding to double layer capacitance; at low potentials, this element may also have a contribution from the mass-transfer process. The inductive loop observed in the LF region of the spectra at lower potentials is due to the relaxation of adsorbed reaction intermediates.³⁵ This inductive feature is modeled using an inductor element (L) along with a series inductive resistance (R_L). With ionomer-containing catalyst layers, a LF semi-circle is also observed along with the (R_1, Q_1) element discussed above. Since the diameter of the LF semi-circle varies with ionomer content and rpm, it is ascribed to the oxygen mass-transfer from the bulk of the electrolyte to the active catalyst sites. This mass-transfer process is represented with an (R_2, Q_2) element in the EC, where R_2 is the mass-transfer resistance (R_d) and the Q_2 is the CPE₂ originating from the diffusion process. With ionomer-containing catalysts, R_p represents the sum of R_{ct} and R_d (R_2). In addition to these features, the carbon-support of the catalyst can also contribute to the EI spectral features (see the section "Effect of carbon-support in the catalyst layer on the EI spectra"). The ionomer-containing carbon spectrum manifests an EDR (45° line in the high frequency (HF) region) and a capacitive behavior (a line almost parallel to the y axis). Therefore, an (R_3, Q_3) element is used to represent the carbon feature in the supported catalysts. But, this feature is present only when both the catalyst and ionomer loadings are high (see the section "Appearance of a HF 45° straight line and two semi-circles"); in the other cases, the carbon feature is not that apparent in the spectrum and it can be neglected in the EC. The solution resistance (R_s) is used in all the spectra and it is obtained from the intercept of the first HF loop on the real axis. More details on CPE elements (Q_1 and Q_2), inductive behavior, and the reasons for their use are discussed in the sections "EIS of ORR on ionomer-free Pt black catalyst layer" and "EIS of ORR on ionomer-containing Pt/C (20 wt%) catalyst layer."

EIS of ORR on ionomer-free Pt black catalyst layer.— The EI spectra of ORR recorded with ionomer-free Pt black in oxygen-saturated 0.1 M HClO_4 solution is shown in Fig. 1. The arc observed in the EI spectrum in the kinetic region (> 900 mV) converges to a semi-circle at lower potentials (Fig. 1a). This is due to the exponential decrease in the interfacial charge-transfer resistance (R_{ct}); the complete spectra are shown in inset to Fig. 1a. In the mixed diffusion-controlled region (~ 850 – 800 mV), along with a LF inductive loop, a semi-circle of decreasing diameter is observed with decrease in potential (Fig. 1b). The diameter of semi-circle indicates the polarization resistance (R_p) of the electrochemical process. In the mass-transport region (~ 725 – 675 mV), an increase in R_p with decrease in potential is evident and a semi-circle with an inductive loop is observed (Fig. 1c). The trend in R_p with potential in the mass-transport region is exactly opposite to that observed in the kinetic and mixed diffusion-controlled regions. This can be due to the higher mass-transfer resistance since the pure charge-transfer resistance should decrease with decrease in electrode potential. The reproducible ORR voltammograms of Pt black (Fig. S1) and the CVs in argon-saturated 0.1 M HClO_4 solution (see inset to Fig. S1 and the relevant discussion

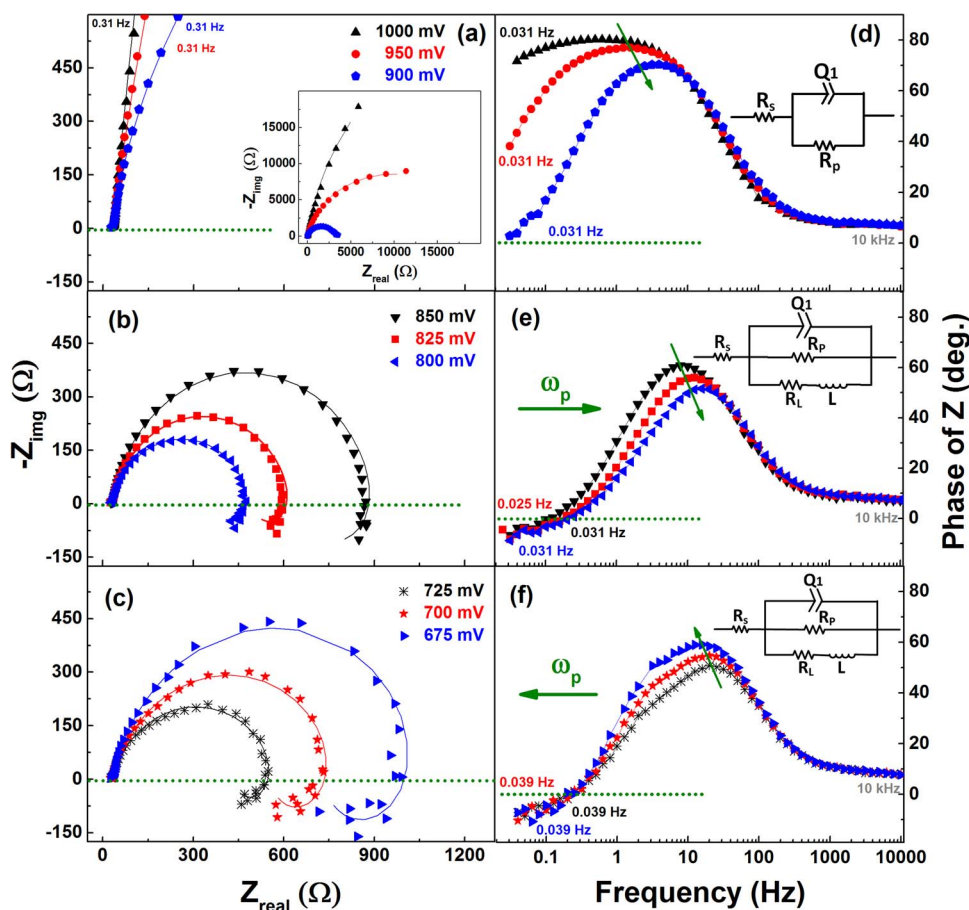


Figure 1. EIS spectra of ORR recorded with ionomer-free Pt black catalyst layer in oxygen-saturated 0.1 M HClO₄ solution at 1600 rpm: (a) kinetic region (1000–900 mV); (b) mixed-diffusion region (850–800 mV); and (c) mass-transport region (725–675 mV). The corresponding Bode phase plots are shown in Fig. 1(d), (e), and (f) along with the respective equivalent circuits (insets). Inset to Fig. 1a show the complete Nyquist plot. The symbols and solid lines show the experimental and the fitted data, respectively.

in SI) suggest that the ionomer-free catalyst layer remains intact even at the end of the experiment.

The phase angle is very high (close to 90°, in the LF region) at high potential (>900 mV) and it starts to decline with decrease in the electrode potential (Fig. 1d). This simple EI spectrum with one time constant, obtained in the kinetic region (>900 mV), can be fitted with a series combination of solution resistance (R_s) and (R_p , CPE₁/Q₁) (R_p and Q elements in parallel) (inset to Fig. 1d). R_p is mainly due to the contribution from the charge-transfer process through the double layer interface. This suggests that, at high potential, the interface behaves like a capacitor. Constant phase element (CPE) is used to fit the experimental data instead of a pure capacitor since the quality of the fit is poor with the latter (see Fig. S2 and the relevant text in SI). The physical reason for replacing capacitor with CPE is well-established in the literature and it is due to the frequency dependence (dispersion) of the measured electrode-electrolyte interfacial capacitance.^{52–55} The CPE behavior is attributed to surface inhomogeneity, roughness, reactivity, porosity, and current and potential distributions associated with the electrode geometry.^{52–55} It cannot be represented by any finite number of equivalent circuit elements and it originates from a surface/normal distribution of time constants over many orders of magnitude.^{26,52–60}

From the value of CPE, the double layer capacitance (C_{dl}) can be estimated using the following formula (equation 1) for the normal distribution (hierarchical structure of elements that form the electrode) of the time constants of electrode elements:^{53,57,61}

$$C_{dl}^{\phi} = \frac{Q}{(R_p^{-1})^{1-\phi}} \quad [1]$$

Where, Q is CPE constant; and ϕ is CPE exponent. Fitting the experimental data with the above-equivalent circuit shows that the value of ϕ is a constant (0.9 ± 0.01) at potential above 900 mV (Fig. S3) and it suggests that the CPE behavior originates from a capacitor.⁵⁴

In the mixed diffusion-controlled region (~850–800 mV), as expected, the characteristic frequency (ω_p) shifts to higher value in the Bode plot (Fig. 1e). In addition to R_s , an inductor (L) along with inductive resistance (R_L) are used parallel to the (R_p , Q) element to fit the experimental data (inset to Fig. 1e). The negative phase angle corresponding to inductive behavior can be observed from the Bode plot shown in Fig. 1e. This LF inductive feature, reported in the EI spectra of ORR, is predicted by the models that account for Pt dissolution or relaxation of the adsorbed intermediates on Pt (Pt-OH_{ads}, Pt-OOH_{ads} and PtO_{ads} (see Pt voltammogram shown in inset to Fig. S1)).^{19,35,62–65} It means that the current signal follows a voltage perturbation with a phase delay (90° for a pure inductor) and it is modeled using an inductor (L). At high frequencies, the inductor has infinite impedance (inductive reactance (X_L) = ωL) and the coverage remains constant; therefore, the current response without change in coverage is decided by R_p . At the zero-frequency limit, since coverage reaches an equilibrium value, an inductive resistance (R_L) is used to modify the current response and it is decided by the parallel combination of R_p and R_L . In the mass-transport region (~725–675 mV), the characteristic frequency (ω_p) is shifted to lower value with decrease in potential, unlike that in the diffusion-controlled region (~850 to 800 mV) (Fig. 1f). In this region, a strong inductive behavior is observed and the impedance spectra are fitted with a series combination of R_s and (R_p , Q₁, R_L /L) elements (inset to Fig. 1f). The total

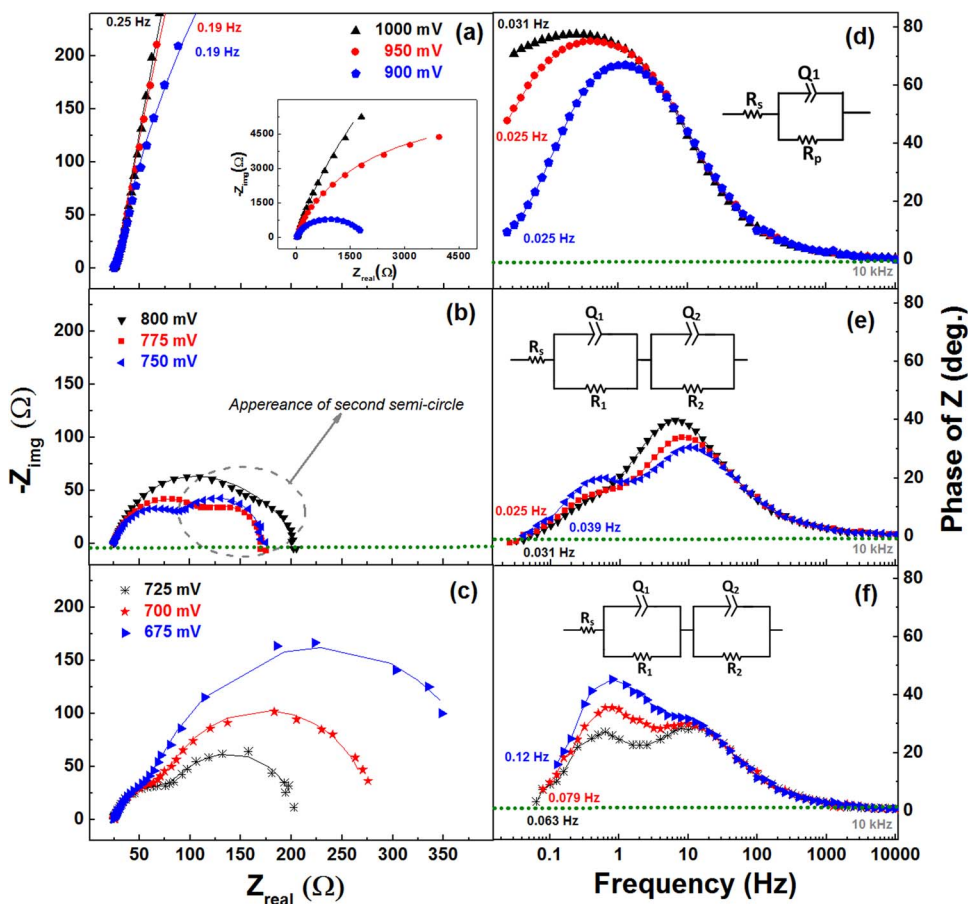


Figure 2. EIS spectra of ORR recorded with Pt/C (20 wt%) catalyst layer with low ionomer content in oxygen-saturated 0.1 M HClO₄ solution at 1600 rpm: (a) kinetic region (1000–900 mV); (b) mixed-diffusion region (800–750 mV); and (c) mass-transport region (725–675 mV). The corresponding Bode phase plots are shown in Fig. 2(d), (e), and (f) along with the respective equivalent circuits (insets). Inset to Fig. 2(a) show the complete Nyquist plot. The symbols and solid lines show the experimental and the fitted data, respectively.

resistance (R_p) of the ionomer-free Pt-black plotted against the applied electrode potential is shown in Fig. S4. R_p decreases with potential down to ~ 0.75 V and it starts to increase gradually with further decrease in potential. This indicates that R_p has contributions from both the charge-transfer and mass-transfer processes. Down to ~ 0.75 V, R_p is dominated by the charge-transfer resistance, and at further lower potentials, it is dominated by the mass-transfer resistance. As discussed below, at a given potential, R_p is found to decrease with increase in rpm and it confirms the above conjecture.

Interestingly, separate semi-circles corresponding to charge-transfer and mass-transfer are not observed in the spectra, perhaps due to the comparable time constants of the two processes or the time constant for one process is smaller than that for the other; thus, fitting the experimental data with two (R, Q) elements, corresponding to the charge-transfer and mass-transfer, along with L and R_L with R_s yields a poor fit (Fig. S5).

Similar observations (only one arc on the Nyquist plot and trend in R_p with potential) were reported by Perez et al. with Pt/C (with a dilute suspension of Teflon emulsion) on thin porous-coated rotating disk electrode (TPC/RDE).³⁹ The impedance response of the electrode was reportedly masked by the very high capacitance which is much larger than what is observed in this study; this may be due to the high Teflon content in the catalysts layer.^{39,40} As discussed below, two semi-circles are observed in the mixed diffusion-controlled region on ionomer-containing catalyst layer.

EIS of ORR on ionomer-free Pt/C (20 wt%) catalyst layer.— The EI spectra of ORR with ionomer-free carbon-supported Pt (20 wt%)

recorded under same conditions (Fig. S6) are similar to that observed with ionomer-free Pt black (Fig. 1). Irrespective of the potential, the EI spectra of ionomer-free Pt black and Pt/C (20 wt%) show only one arc/semi-circle on the Nyquist plot; spectrum is not resolved from the charge-transfer and mass-transfer processes on the Nyquist plot due to the comparable time constants of the two processes or the time constant for one process is smaller than that of the other. Therefore, similar equivalent circuits with only one (R, Q) element in series with R_s are used to fit the experimental data at different potential regions. But, the inductive behavior in the mixed diffusion-controlled region is not that prominent with Pt/C catalyst (Fig. S6(b)), unlike that observed with ionomer-free Pt black (Fig. 1e).

EIS of ORR on ionomer-containing Pt/C (20 wt%) catalyst layer.— The EI spectra of Pt/C (20 wt%) catalyst layer with low-ionomer content are shown in Fig. 2. In the kinetic region, the EI spectrum (Fig. 2a) is similar to that of ionomer-free Pt black; the complete spectra are shown in inset to Fig. 2a. In the mixed diffusion-controlled region, a LF semi-circle starts to appear on the Nyquist plot (Fig. 2b). The appearance of the LF semi-circle is evident at 775 and 750 mV. This is unlike the case with ionomer-free catalyst layer with both Pt black and Pt/C (20 wt%). The LF semi-circle appears even with minute quantity of ionomer in the thin-film catalyst layer. In the mass-transport region at 675 mV, the diameter of the LF semi-circle increases further and it merges almost with the HF semi-circle (Fig. 2c). The charge-transfer resistance is almost negligible and the spectrum is dominated by the mass-transfer process. In kinetic region, the Bode plot (Fig. 2d) is similar to that obtained with ionomer-free Pt black

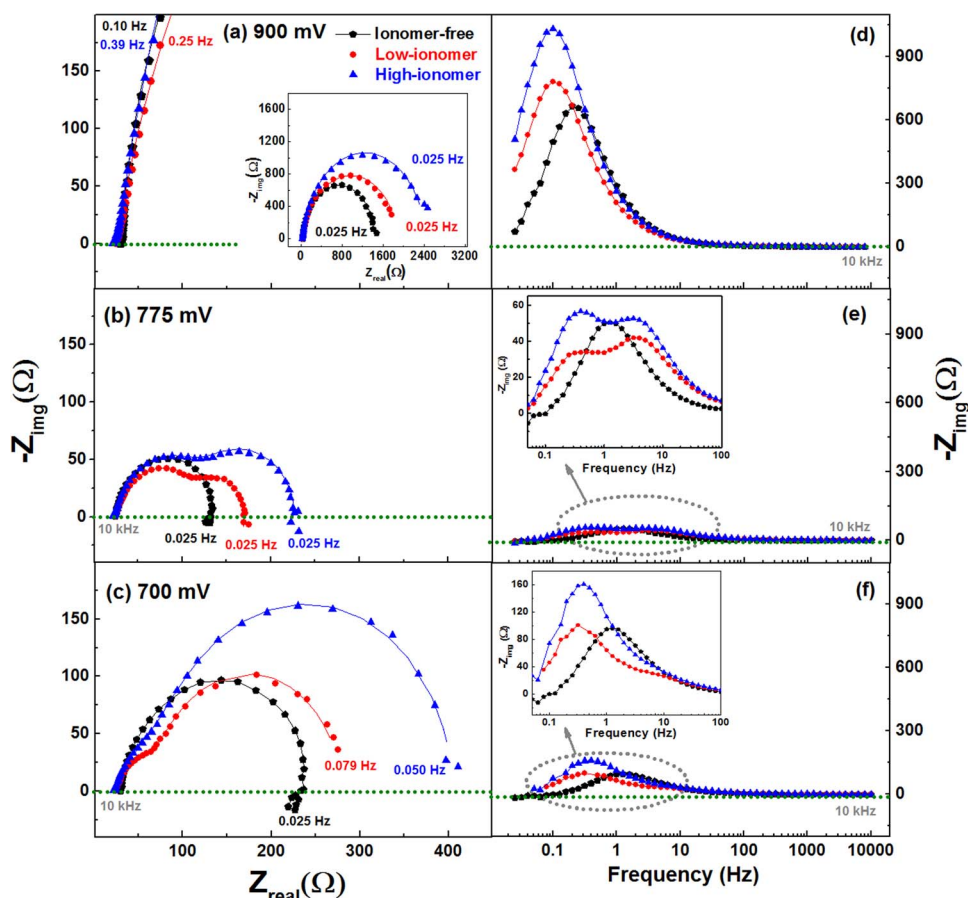


Figure 3. EI spectra of ORR recorded with 20 wt% Pt/C (with ionomer-free, low and high ionomer content in the catalyst layer) in oxygen-saturated 0.1 M HClO₄ solution at 1600 rpm: (a) kinetic region (900 mV); (b) mixed diffusion-controlled region (775 mV); and (c) mass-transport region (700 mV). The corresponding Bode plots of the imaginary component of impedance are shown in Fig. 3(d), (e), and (f). The symbols and solid lines show the experimental and the fitted data, respectively. Inset to Fig. 3(a) shows the complete Nyquist plot and insets to Fig. 3 (e) and (f) show the corresponding magnified view of Bode plots.

(Fig. 1d). The equivalent circuit (inset to Fig. 2d) is similar to that used with ionomer-free catalyst layers discussed above (Fig. 1d) in this potential regime. In the mixed diffusion-controlled region, the minor hump observed in the LF region of the Bode plot corresponds to the LF semi-circle on the Nyquist plot (Fig. 2e). In this region, the equivalent circuit with a series combination of R_s and two (R , Q) elements (high-frequency (R_1 , Q_1) and low-frequency (R_2 , Q_2)) is used to fit the experimental data (see inset to Fig. 2e). The HF (R_1 , Q_1) element is associated with the charge-transfer process through electrode-electrolyte interface and the LF (R_2 , Q_2) element can be attributed to the O₂ mass-transport.⁶⁶ The inductive behavior is not prominent in these spectra, unlike those of ionomer-free Pt black (see Fig. 1e). These spectral features depend on the metal loading, carbon-support loading, and ionomer content in the catalyst layer and their origin is discussed in the following sections.

In the mass-transport region, the dominance of the mass-transfer resistance is evident from the Bode plot shown in Fig. 2f. The HF semi-circle is almost constant and the LF semi-circle due to mass-transport increases with further decrease in potential; the spectra in this region is fitted with the two (R , Q) elements shown in the inset to Fig. 2f.

The impedance spectra consisting of two capacitive loops and one LF inductive loop was reported by Antoine et al. with Pt nanoparticles on porous gas diffusion electrode (GDE) in PEFC configuration.³⁵ These loops were attributed to ionic ohmic drop/double layer charging inside the active layer, charge-transfer, and relaxation of adsorbed-oxygenated species. Whereas, Ciureanu et al. reported two semi-circles on the Nyquist plot and attributed the HF semi-circle to the charge-transfer process through double layer capacitor (C_{dl} - R_{ct}) and

LF semi-circle to the diffusion through the backing.²⁶ With our catalysts, the HF semi-circle observed is due to the charge-transfer process (diameter of the semi-circle is a function of potential).

Effect of the ionomer content in the catalyst layer on the EI spectra.— The impedance spectra of the Pt/C (20 wt%) with different ionomer contents are compared in Fig. 3 (see details on ink preparation given in SI for catalyst layer with low/high-ionomer contents). In the kinetic region (900 mV), at a given potential, the features of the EI spectra with the ionomer-free catalyst layer are similar to that of the ionomer-containing catalyst layer (Fig. 3a). In this region, the spectrum consists of an arc or semi-circle and its diameter decreases with decreasing potential. At a given potential, the diameter of the semi-circle increases with increase in ionomer content in the catalyst layer and it is in the order of Pt/C (high ionomer content) > Pt/C (low ionomer content) > ionomer-free Pt/C (inset to Fig. 3a).

In the mixed diffusion-controlled region, the impedance spectra of ionomer-free Pt/C show only one semi-circle on the Nyquist plot (Fig. S6). At the same time, the spectra of ionomer-containing Pt/C consist of two semi-circles (Fig. 3b). At a given potential, the diameter of the LF semi-circle of the catalyst layer with high ionomer content is higher than that of the catalyst layer with low ionomer content, may be due to the increase in mass-transfer resistance. At the same time, in this potential regime, the diameter of the HF semi-circle is less than that of the LF semi-circle and it indicates the dominance of diffusion resistance when compared to the charge-transfer resistance. To confirm the origin of the LF semi-circle, EI spectra of ionomer-containing Pt black with carbon was recorded (Fig. S7). The presence of LF semi-circle confirms that it originates only in the presence of ionomer in the

catalyst layer (see Fig. 3); in the mass-transport region, the spectra of ionomer-free catalyst layer consist of a slightly distorted semi-circle (Fig. 3c). The features of low and high ionomer content catalyst layers are comparable (Fig. 2 and Fig. S8). Thus, the presence of ionomer helps to resolve both the kinetic and mass-transport processes. The ionomer content in the catalyst layer reduces the double layer capacitance (see Tables S1, S2 and S3) and the extra ionomer mass-transport resistance adds to R_p (see Fig. 3). The reduction in capacitance shifts the kinetic process to higher frequencies and the increase in R_p helps to resolve the kinetic process. Moreover, the oxygen storage capacity of the thin-ionomer film is not sufficient to account for the observed capacitance of the LF semi-circle (see calculation shown in section S2 of SI) even with ca. 30 times more oxygen storage per volume of gas-filled pores relative to that of the electrolyte-filled pores. Therefore, the LF semi-circle is attributed to external mass-transport, a process which is significant regardless of ionomer content (see Fig. 3d below). With ionomer-free catalyst layer, it seems that the HF semi-circle is hidden by the much larger LF semi-circle (this is perhaps the case with ionomer-free catalyst layer, where only one semi-circle is observed (see the Fig. 3d). The external oxygen storage contributes only to the external mass-transport time constant and any internal oxygen storage will contribute to both time constants. Therefore, the external mass transport will have a lower characteristic frequency than the internal mass transport. Thus, the addition of ionomer only causes separation of the time constants of the charge-transfer and external mass-transfer processes and it does not develop a new LF semi-circle.

The corresponding Bode plots of the imaginary component of impedance are shown in the Fig. 3d, 3e, and 3f; these plots are helpful to illustrate the characteristic frequency in case of series equivalent circuits than the Bode phase plots because the phase is affected by any series impedance. In the kinetic region, only one characteristic peak is observed with all the catalyst layers and it is at the LF region (see Fig. 3d). In the mixed-diffusion controlled region, two characteristic peaks are observed with ionomer-containing catalyst layers. The LF peak corresponding to mass-transfer is shifted to further LF region compared to that of the ionomer-free catalyst layer (see Fig. 3e and the explanation for the separation of time constants); the inset to the Fig. 3e shows the magnified view of the spectrum. In the mass-transport region, the ionomer-free catalyst layer shows only one peak on the Bode plot; may be due to the overlap between the kinetic and the mass-transport processes. With ionomer-containing catalysts layer, two distinguishable peaks are observed (see Fig. 3f and inset to Fig. 3f). The second peak at the LF region is more apparent compared to that of the mixed-diffusion controlled region.

With increase in the ionomer content in the catalyst layer, the activity of the catalyst decreases as observed from the ORR voltammograms (Fig. S9); but, the electrochemically active surface area increases (Table S4). Moreover, the decrease in the limiting current with increase in ionomer loading in the catalyst layer can be explained by the extra ionomer mass-transport resistance (see Tables S1, S2, and S3 and Fig. 3). The extra mass-transport resistance must be internal to the film, not external, and the internal mass-transport resistance shows a more gradual approach to the limiting current density (as seen from Fig. S9). It would also be appropriate to compare ORR voltammograms (background and IR-corrected) normalized with the electrochemical surface area (ESA) of the catalyst layer. These voltammograms show that the internal mass-transport resistance yields a gradual approach to mass-transfer limiting current density (see inset to the Fig. S9).

Effect of carbon-support in the catalyst layer on the EI spectra.—

EI spectra of carbon (ionomer-free and ionomer-containing) are recorded in the same electrolyte to investigate the effect of carbon-support in the catalyst layer. The EI spectrum of ionomer-free carbon shows features similar to that of a porous carbon electrode at all the potentials under investigation (Fig. 4). It shows the typical carbon electrochemical capacitor features with equivalent series resistance (ESR) and equivalent distributed resistance (EDR) (Fig. 4a).⁶⁷ The observed EDR is $\sim 3 \Omega\text{-cm}^2$ (see Fig. 4), which is comparable to that

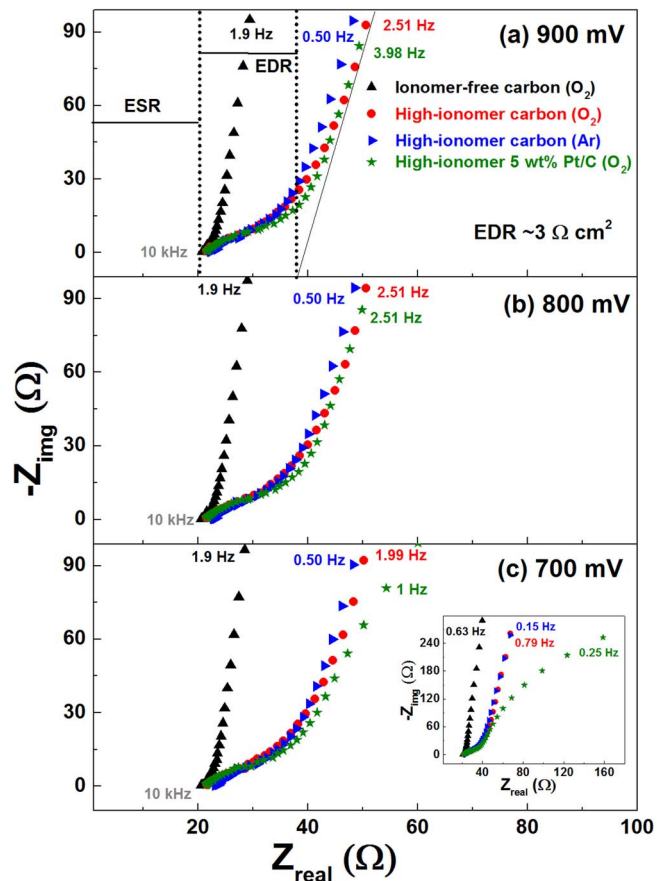


Figure 4. EI spectra of ionomer-free carbon, high ionomer content carbon and carbon-supported Pt (5 wt%) with high ionomer content in the catalyst layer recorded in oxygen-saturated 0.1 M HClO₄ solution at 1600 rpm: (a) kinetic region (900 mV), (b) mixed diffusion-controlled region (800 mV), and (c) mass-transport region (700 mV). EI spectra of high-ionomer containing carbon recorded in argon-saturated 0.1 M HClO₄ are also included. Inset to the Fig. 4(c) shows the complete Nyquist plot at 700 mV.

estimated with a carbon loading of 0.3 mg cm^{-2} (corresponding to an electrode thickness of $\sim 10 \mu\text{m}$). Therefore, the effective conductivity of the ionomer-containing porous electrode, soaked in 0.1 M HClO₄, is $\sim 1 \times 10^{-4} \text{ S cm}^{-1}$ (similar values are observed with typical PEFC electrode).^{68,69}

Spectrum of ionomer-free carbon is almost parallel to the y-axis but with a minor tilt toward the x-axis. The Bode plot in the LF region is parallel to the x-axis with a constant phase angle of $\sim 80^\circ$ (Fig. S10); the very high phase angle is attributed to the highly capacitive nature of carbon; it is also evident from the CVs shown in Fig. S11 (a) (rectangular double layer feature with minor parasitic reactions). With ionomer-containing (high) carbon film, the spectrum changes drastically. There is an extended line with 45° tilt (relative to that of ionomer-free carbon), and at lower frequencies, it turns almost parallel to the y-axis. These features are present even in argon-saturated electrolyte; therefore, the above-mentioned features are not due to oxygen diffusion limitations (Fig. 4b). Moreover, the features of oxygen diffusion limitation appear at the LF regime in the EI spectrum of ORR. The other mass-transfer limitation that is possible is that of the H⁺ ions. Thus, the extended line with 45° tilt (Warburg behavior) is a consequence of the H⁺ ion transport limitations through the distributed resistance/capacitance in the porous carbon electrode,^{23,25,67} note that carbon is hydrophobic and Nafion ionomer conductivity is poor at room temperature.

The EIS data with Pt/C (5 wt% with high-ionomer content) is also included for comparison in Fig. 4. The corresponding CVs and ORR voltammograms recorded prior to the EI measurement are shown

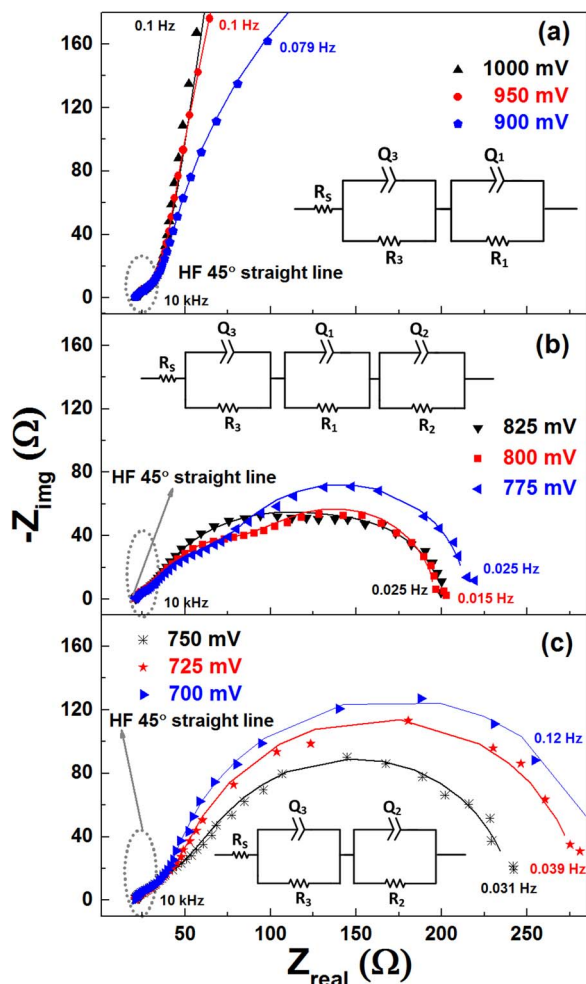


Figure 5. EIS spectra of ORR recorded with Pt/C (20 wt%; $50 \mu\text{g cm}^{-2}$) catalyst layer with high ionomer content recorded in oxygen-saturated 0.1 M HClO_4 solution at 1600 rpm: (a) kinetic region (1000–900 mV); (b) mixed diffusion-controlled region (825–775 mV); and (c) mass-transport region (750–700 mV). The corresponding equivalent circuits are shown in insets to Fig. 5(a), (b), and (c). The symbols and solid lines show the experimental and the fitted data, respectively.

in Fig. S11 (a) and (b), respectively. The EIS spectra of ionomer-containing Pt/C (5 wt%) are comparable to that of ionomer-containing carbon at 900 and 800 mV. But at lower potentials (≥ 700 mV), the vertical line converges to a semi-circle; the line with 45° tilt in the HF region is still present (Fig. 4c and inset to Fig. 4c). With increase in Pt content in the catalyst (decrease in carbon content), the line with 45° tilt in the HF region gets suppressed (Fig. 2). With Pt black, it is completely absent and only pure Pt features are observed (Fig. 1a). This is due to the fact that the onset potential of ORR on carbon is at much lower potential as compared with that of Pt/C (5 wt%) (Fig. S11 (a) and (b)). These experiments with ionomer-free and ionomer-containing catalyst layers of various Pt and carbon contents help to resolve correctly every minute feature of the spectra in a RDE configuration. The spectrum of carbon with Nafion helps to reduce the complexity of assigning the underlying physical processes.

Appearance of a HF 45° straight line and two semi-circles.— The EIS spectra of ORR on catalyst layer containing Pt/C (20 wt%) with high catalyst loading ($50 \mu\text{g cm}^{-2}$) and high ionomer content are shown in Fig. 5.

In the kinetic region (>900 mV; (Fig. 5a)), the impedance spectra consists of a 45° HF straight line and a LF arc; unlike that of Pt/C or ionomer-free Pt black (Figs. 1 and 2). The spectrum is fitted with two

(R, Q) elements in this region (see inset to Fig. 5a). The HF (R_3 , Q_3) element is related to the proton diffusion limitation in carbon/Nafion matrix^{23,25} and the LF (R_1 , Q_1) element is related to the charge-transfer process through the double layer interface.

In the mixed diffusion-controlled region (825–775 mV), in addition to the two (R, Q) elements discussed in the kinetic region, a LF semi-circle is also observed on the Nyquist plot (Fig. 5b) due to the external mass-transport of the oxygen as discussed above (discussion of Fig. 3). The spectrum in this region is fitted with three (R, Q) elements in series with the solution resistance R_s (see inset to the Fig. 5b). Similar observations were reported by Springer et al. and they proposed that the 45° straight line may be due to the transport limitations of H^+ ions.²⁵ This feature (45° straight line), which is evident on electrodes with high catalyst loading ($50 \mu\text{g cm}^{-2}$), is absent in the spectra recorded with ionomer-free Pt black and it is not so apparent with electrodes of low catalyst loading (Pt/C 20 wt%) (the catalyst loading has been increased purposefully to magnify the 45° straight line (encircled part in Fig. 5)). With thicker catalyst layers, the hydrophobic carbon may contribute to the diffusion limitations of the H^+ ions (see also the discussion on carbon spectra (Fig. 4)).

In the mass-transport region, the charge-transfer resistance further decreases and hence a single semi-circle representing both the charge-transfer and mass-transfer resistances appears with major contribution from the latter (Fig. 5c). The spectra in this region is fitted with two (R, Q) element along with the series resistance R_s ; the charge-transfer process (R_1 , Q_1) element is removed from the equivalent circuit (inset to the Fig. 5c).

With ionomer-free catalyst layers, the LF semi-circle and the HF arc are not observed over the whole range of potential (~ 950 to 675 mV) (Fig. 1). The only arc/semi-circle observed can be attributed to the charge-transfer process. On catalyst layer with lower loading ($\sim 15 \mu\text{g cm}^{-2}$) of the catalyst and ionomer, only two semi-circles are observed and the HF arc is not so apparent; may be masked by the other features. With increase in the catalyst loading (from 15 to $50 \mu\text{g cm}^{-2}$) and ionomer content a HF 45° straight line feature is observed. Thus, as discussed above (Fig. 5), the use of different equivalent circuits to fit the EIS spectra is justified.

Effect of rotation rate (rpm) on EIS spectra of ORR.— The dependence of EIS spectra on rpm at 875 mV on ionomer-free Pt/C (20 wt%) catalyst is shown in the Fig. 6a. The impedance spectrum consists of only one semi-circle on the Nyquist plot. At 2000 rpm, the diameter of the semi-circle is lowest and it is highest at 800 rpm. This suggests that mass-transfer affects the catalytic activity even in the kinetic region. To extract the pure charge-transfer resistance in the kinetic region, the plot of R_p vs. $\omega^{-0.5}$ is extrapolated to infinite rotation rate (at 0 on $\omega^{-0.5}$ axis). From the intercept on y-axis, the pure charge-transfer resistance is estimated. The effect of R_p , R_{ct} , and R_d on the rotation rate is shown in the inset to Fig. 6a. In this region, R_p is dominated by the charge-transfer resistance at higher rpm. In the mixed diffusion-controlled region (750 mV), the EIS spectra consist of a depressed semi-circle (Fig. 6b); this may be due to a superimposition of two capacitive loops. Even at very low rpm, where the mass transfer effect dominates, the two semi-circles are not well-resolved, unlike that observed with ionomer-containing catalysts. Perhaps, the time constants of charge-transfer and mass-transfer are comparable or the time constant for one process is smaller than that of the other. The R_p obtained from the CNLS fit is plotted as a function of the rpm and it gradually decreases with increase in the rpm. In this region, R_p is dominated by the R_d (inset to Fig. 6b).

On ionomer-containing Pt/C (20 wt%) catalyst layers, in the kinetic region at 875 mV (Fig. 6c), the effect of rpm is more prominent, i.e., there is higher increase in R_p with decrease in rpm (relative to ionomer-free catalyst layer) (inset to Fig. 6c). This suggests that the mass-transfer effect contributes to the R_p even at higher potential; thus, ionomer content affects the measured ORR activity. Hence, the Nyquist plots, depicting the effect of ionomer content, help researchers to optimize the catalyst layer composition in the fuel cell operating

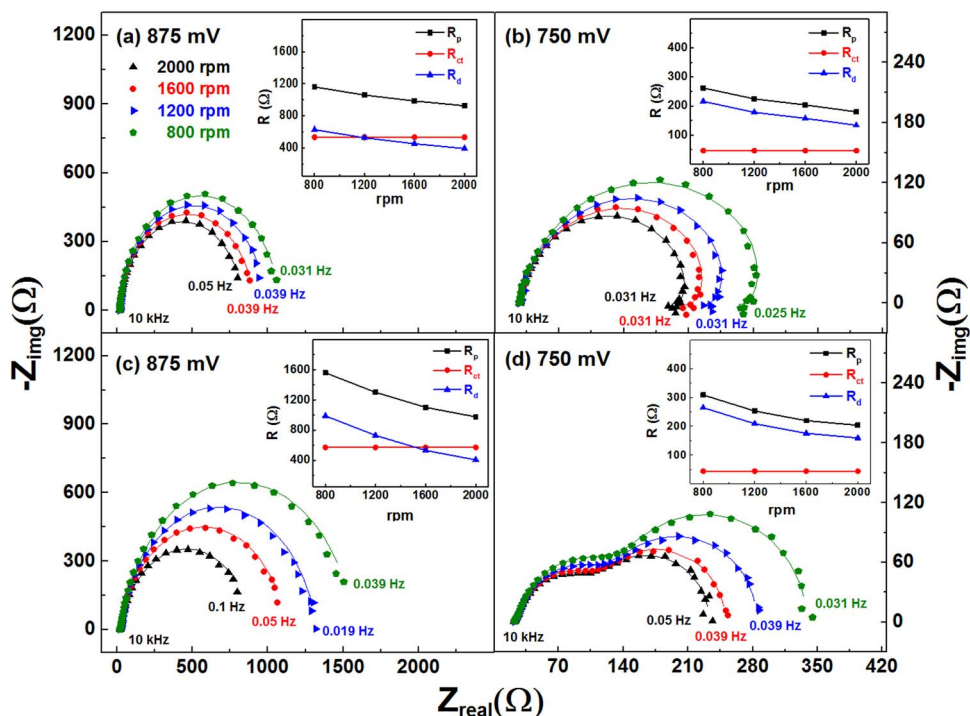


Figure 6. EI spectra of ORR recorded with thin-film catalyst layer composed of ionomer-free Pt/C (20 wt%) (Fig. 6(a) and (b)) and ionomer-containing Pt/C (20 wt%) (Fig. 6(c) and (d)) in oxygen-saturated 0.1 M HClO₄ solution with 2000, 1600, 1200, and 800 rpm. Insets to Fig. 6(a), (b), (c) and (d) show the plot of R_p , R_{ct} and R_d as a function of rpm. The symbols and solid lines show the experimental and the fitted data, respectively.

condition. The EI spectrum in the mixed diffusion-controlled region at 750 mV is shown in Fig. 6d. Two semi-circles are observed on the Nyquist plot. From the CNLS fit, R_p and diffusion resistance (R_d) are estimated and plotted as function of rpm (inset to Fig. 6d). Both R_p and R_d decrease with increase in rpm. R_p is dominated by the R_d and it suggests the strong contribution of mass-transfer to the polarization resistance. These results are in line with that reported by Ciureanu et al. wherein increase in the air flow rate decreases the R_p and R_d in PEFC configuration.²⁶ The presence of a LF arc/semi-circle with ionomer-containing catalyst layer and the strong dependence of its diameter on rpm suggest that the LF arc is due to the external mass-transport limitation of O₂. The thickness of the Nafion ionomer in the catalyst layer ranges from ~30 nm (low-ionomer) to ~150 nm (high-ionomer). Thus, in RDE configuration, the impedance features can be conclusively attributed to specific electrode processes.

Kinetic parameters.— Exchange current density (j_o).— The exchange current density (j_o), that decides the quality of the catalyst, is the current that flows at the equilibrium condition for a redox reaction. In the open circuit condition, it is estimated from the R_{ct} obtained by fitting the EI spectra. But, as discussed earlier, estimation of the pure charge-transfer resistance (R_{ct}) is difficult even in the kinetic region because of the influence of mass-transfer effects and platinum surface oxidation. Thus, the exchange current density j_o is calculated by extrapolating R_p to the reversible thermodynamic potential of ORR (i.e. 1.229 V) (Fig. S12); further details are shown in section S2 of SI. The j_o estimated from the extrapolation is 1.28×10^{-10} A cm⁻² and it is comparable to that reported in the literature.³⁹

Tafel plot of ionomer-free Pt black.— Tafel curve (Fig. 7) is generated by plotting the polarization resistance ($\log R_p^{-1}$) vs. the IR-corrected cathode potential; R_p is obtained from the impedance data using the CNLS fitting (Fig. 1). The Tafel plot shows two different regions/slopes as a function of potential. At potential above >0.86 V (V_1), a slope of ~64 mV/decade is observed, and in the range of ~0.86 to 0.76 V (V_1 to V_2), a slope of ~125 mV/decade is observed. A slope of ~250 mV/decade is observed below ~0.75 V (V_2) due

to the mass-transport limitation; for convenience, this is not shown in the Tafel plot. Similar type of the Tafel behavior is reported in the literature^{26,37,38} and the Tafel slope are comparable to that reported from the DC measurements.^{70–71}

Diffusion coefficient of oxygen in ionomer-containing catalyst layer.— Though the LF semi-circle is apparent only in the presence of ionomer in the catalyst layer, it is attributed to the external mass-transport process (see discussion on Fig. 3). Moreover, the LF semi-circle has contributions from kinetic, external and internal mass-transport processes and there is no clear Warburg feature in the spectrum. Therefore, it is not appropriate to estimate the diffusion coefficient of oxygen through the thin-film of ionomer from the LF semi-circle.

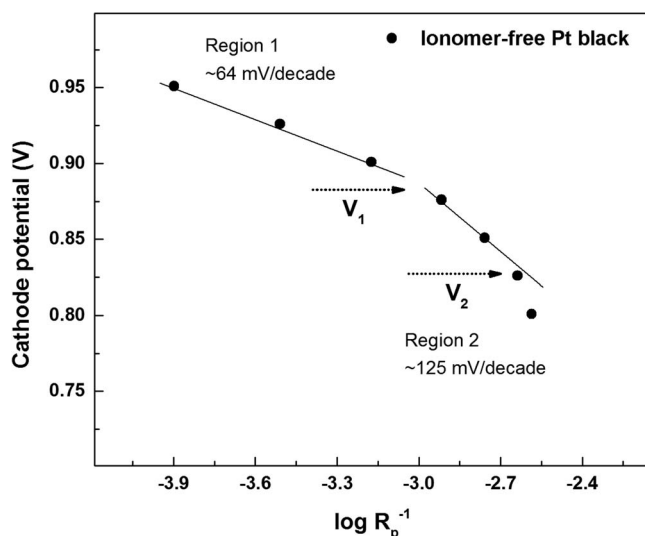


Figure 7. Tafel plot of ORR with ionomer-free Pt black in 0.1 M HClO₄ solution.

ESA calculation.—The capacitance calculated (using equation 1) can be used to estimate the ESA. The double layer capacitance (C_{dl}^0) of 1 cm² Pt in liquid electrolyte at 0.9 V is 60 μF cm⁻².^{26,72} The measured capacitance of Pt black is ~20 F g⁻¹ and the corresponding ESA is ~33 m² g⁻¹. The ESA of the catalysts (Table S5) estimated from the EIS is in line with that obtained from the voltammetric measurement (H_{upd} region of the CV) (see details on section S2 in SI).^{73,74}

Conclusions

EI spectra of ORR on unsupported and carbon-supported Pt (with different metal contents; 5 and 20 wt%) with or without ionomer are investigated in acidic media in a TF-RDE configuration. The nature of the ORR impedance spectra depends on the applied potential and on the thin-film catalysts layer constituents. The simplest spectrum of ORR consisting of an arc/semi-circle is obtained with ionomer-free Pt/C and Pt black at high potential (>900 mV). The polarization resistance decreases with decrease in potential till ~750 mV, and it increases with further decrease in potential. At higher potentials, the polarization resistance is dominated by the charge-transfer process and at lower potentials it is dominated by the mass-transfer process. With introduction of ionomer in the catalyst layer, a LF semi-circle appears due to the separation of the time constants of the charge-transfer and mass-transfer processes. The LF semi-circle due to the external mass-transport of O₂ is observed along with the HF semi-circle due to the charge-transfer process across the double layer; this is further confirmed by varying the ionomer content in the thin-film catalyst layer. The separation of the time constants of two processes (charge-transfer and mass-transfer) is attributed to the extra oxygen storage in the diffusion layer, decrease in the double layer capacitance and increase in the polarization resistance with ionomer content. The HF 45° straight line is attributed to the protonic diffusion limitation through the relatively thick hydrophobic carbon/Nafion matrix; this feature is not evident on ionomer-free catalyst layers.

An inductive loop due to adsorption of surface impurities appears in the LF region of the spectrum and it is prominent with ionomer-free Pt black, suggesting the formation of oxides even at lower potentials. The kinetic parameters (Tafel slope, charge-transfer resistance, and exchange current density) and ESA are estimated. To the best of our knowledge, this is the first report on EIS of ORR on Pt-based catalysts in RDE configuration (in the absence of porous gas diffusion media) that shows close resemblance with fuel cell EI spectra. EIS technique on TF-RDE using a minute amount of catalyst can be effectively used to characterize emerging new catalyst formulations, particularly, materials including non-precious metal catalysts of low turnover frequency (TOF).

Acknowledgments

Department of Science and Technology (DST), India, is acknowledged for the financial support of the project through the grant (SR/S1/PC-68/2012).

List of Symbols

A	Geometrical area of the electrode, cm ²
C _o	Concentration of the oxygen, mol cm ⁻³
C _{dl}	Double layer capacitance, F
ESR	Equivalent series resistance, Ω
EDR	Equivalent distributed resistance, Ω
F	Faraday constant, C mol ⁻¹
j _o	Exchange current density, A cm ⁻²
L	Inductor, H
n	Number of electron transferred
Q ₁	Constant phase element representing the double layer, S-s ^φ
Q ₂	Constant phase element due to external mass-transport, S-s ^φ
Q ₃	Constant phase element in the agglomerate carbon/Nafion matrix, S-s ^φ

R	Universal gas constant, J mol ⁻¹ K ⁻¹
R ₁	Charge transfer resistance, Ω
R ₂ /R _{dl}	Resistance due to external mass-transport, Ω
R ₃	Diffusion resistance due to carbon/Nafion matrix, Ω
R _{ct}	Charge transfer resistance, Ω
R _L	Inductive resistance due to adsorption process, Ω
R _p	Polarization resistance of ionomer-free Pt black and Pt/C (20 wt%), Ω
R _s	Solution resistance, Ω
T	Temperature, K
Z _{CPE}	Impedance of the constant phase element, Ω
Z _w	Impedance of Warburg element, Ω
φ	Constant phase element exponent
σ	Warburg coefficient, Ω s ^{-0.5}

References

- H. A. Gasteiger, S. S. Kocha, B. Sompalli, and F. T. Wagner, *Appl. Catalysis B: Environ.*, **56**, 9 (2005).
- T. J. Schmidt, U. A. Paulus, H. A. Gasteiger, N. Alonso-Vante, and R. J. Behm, *J. Electrochem. Soc.*, **147**, 2620 (2000).
- O. Savadogo, K. Lee, K. Oishi, S. Mitsushima, N. Kamiya, and K. -i. Ota, *Electrochem. Commun.*, **6**, 105 (2004).
- G. Wu, K. L. More, C. M. Johnston, and P. Zelenay, *Science*, **332**, 443 (2011).
- M. Lefèvre, E. Proietti, F. Jaouen, and J.-P. Dodelet, *Science*, **324**, 71 (2009).
- H. A. Gasteiger and N. M. Markovic, *Science*, **324**, 48 (2009).
- F. Jaouen, E. Proietti, M. Lefevre, R. Chenitz, J.-P. Dodelet, G. Wu, H. T. Chung, C. M. Johnston, and P. Zelenay, *Energy Environ. Sci.*, **4**, 114 (2011).
- J. R. C. Salgado, E. Antolini, and E. R. Gonzalez, *Appl. Catal., B*, 2005, **57**, 283.
- A. K. Shukla, M. Neergat, P. Bera, V. Jayaram, and M. S. Hegde, *J. Electroanal. Chem.*, **504**, 111 (2001).
- M. Neergat, A. K. Shukla, and K. S. Gandhi, *J. Appl. Electrochem.*, **31**, 373 (2001).
- C. O. Laoire, S. Mukerjee, K. M. Abraham, E. J. Plichta, and M. A. Hendrickson, *J. Phys. Chem. C*, **114**, 9178 (2010).
- S. Meini, N. Tsiouvaras, K. U. Schwenke, M. Piana, H. Beyer, L. Lange, and H. A. Gasteiger, *Phys. Chem. Chem. Phys.*, **15**, 11478 (2013).
- Y.-C. Lu, H. A. Gasteiger, and Y. Shao-Horn, *J. Am. Chem. Soc.*, **133**, 19048 (2011).
- X. Ren, S. S. Zhang, D. T. Tran, and J. Read, *J. Mater. Chem.*, **21**, 10118 (2011).
- R. K. Singh, R. Rahul, and M. Neergat, *Phys. Chem. Chem. Phys.*, **15**, 13044 (2013).
- T. E. Springer, T. A. Zawodzinski, and S. Gottesfeld, *J. Electrochem. Soc.*, **138**, 2334 (1991).
- T. E. Springer, M. S. Wilson, and S. Gottesfeld, *J. Electrochem. Soc.*, **140**, 3513 (1993).
- T. A. Zawodzinski Jr., T. E. Springer, F. Uribe, and S. Gottesfeld, *Solid State Ionics*, **60**, 199 (1993).
- P. Pielak, R. Fields, and P. Zelenay, *J. Electrochem. Soc.*, **153**, A1902 (2006).
- T. E. Springer and I. D. Raistrick, *J. Electrochem. Soc.*, **136**, 1594 (1989).
- I. D. Raistrick, *J. Electrochim. Acta*, **35**, 1579 (1990).
- M. Eikerling and A. A. Kornyshev, *J. Electroanal. Chem.*, **453**, 89 (1998).
- M. Eikerling and A. A. Kornyshev, *J. Electroanal. Chem.*, **475**, 107 (1999).
- A. A. Kulikovskiy and M. Eikerling, *J. Electroanal. Chem.*, **691**, 13 (2013).
- T. E. Springer, T. A. Zawodzinski, M. S. Wilson, and S. Gottesfeld, *J. Electrochem. Soc.*, **143**, 587 (1996).
- M. Ciureanu and R. Roberge, *J. Phys. Chem. B*, **105**, 3531 (2001).
- S. J. Lee, S. Mukerjee, J. McBreen, Y. W. Rho, Y. T. Kho, and T. H. Lee, *Electrochim. Acta*, **43**, 3693 (1998).
- F. Capitanio, S. Siracusano, A. Stassi, V. Baglio, A. S. Arico, and A. C. Tavares, *Int. J. Hydrogen Energy*, **39**, 8026 (2014).
- A. Parthasarathy, B. Dave, S. Srinivasan, A. J. Appleby, and C. R. Martin, *J. Electrochem. Soc.*, **139**, 1634 (1992).
- E. Antolini, L. Giorgi, A. Pozio, and E. Passalacqua, *J. Power Sources*, **77**, 136 (1999).
- L. Giorgi, E. Antolini, A. Pozio, and E. Passalacqua, *Electrochim. Acta*, **43**, 3675 (1998).
- S. Holdcroft, *Chem. Mater.*, **26**, 381 (2014).
- C. Paganin, C. L. F. Oliveira, E. A. Ticianelli, T. E. Springer, and E. R. Gonzalez, *Electrochim. Acta*, **43**, 3761 (1998).
- N. Wagner, W. Schnurnberger, B. Muller, and M. Lang, *Electrochim. Acta*, **43**, 3785 (1998).
- O. Antoine, Y. Bultel, and R. Durand, *J. Electroanal. Chem.*, **499**, 85 (2001).
- L. Genies, Y. Bultel, R. Faure, and R. Durand, *Electrochim. Acta*, **48**, 3879 (2003).
- A. Damjanovic and V. Brusice, *Electrochim. Acta*, **12**, 615 (1967).
- D. B. Sepa, M. V. Vojnovic, and A. Damjanovic, *Electrochim. Acta*, **26**, 781 (1981).
- J. Perez, E. R. Gonzalez, and E. A. Ticianelli, *J. Electrochem. Soc.*, **145**, 2307 (1998).
- J. Perez, E. R. Gonzalez, and E. A. Ticianelli, *Electrochim. Acta*, **44**, 1329 (1998).
- J. Perez, A. A. Tanaka, E. R. Gonzalez, and E. A. Ticianelli, *J. Electrochem. Soc.*, **141**, 431 (1994).
- M. Neergat, V. Gunasekar, and R. K. Singh, *J. Electrochem. Soc.*, **158**, B1060 (2011).
- C. H. Choi, S. H. Park, and S. I. Woo, *Phys. Chem. Chem. Phys.*, **14**, 6842 (2012).
- K. Lee, O. Savadogo, A. Ishihara, S. Mitsushima, N. Kamiya, and K. -i. Ota, *J. Electrochem. Soc.*, **153**, A20 (2006).

45. S. Maheswari, P. Sridhar, and S. Pitchumani, *Electrochem. Commun.*, **26**, 37 (2013).
46. N. Alexeyeva, A. Sarapuu, K. Tammeveski, F. J. Vidal-Iglesias, J. Solla-Gullón, and J. M. Feliu, *Electrochim. Acta*, **56**, 6702 (2011).
47. H. Erikson, M. Liik, A. Sarapuu, M. Marandi, V. Sammelselg, and K. Tammeveski, *J. Electroanal. Chem.*, **691**, 35 (2013).
48. R. Rizo, E. Herrero, and J. M. Feliu, *Phys. Chem. Chem. Phys.*, **15**, 15416 (2013).
49. N. M. Markovic, R. R. Adzic, B. D. Cahan, and E. B. Yeager, *J. Electroanal. Chem.*, **377**, 249 (1994).
50. U. A. Paulus, T. J. Schmidt, H. A. Gasteiger, and R. J. Behm, *J. Electroanal. Chem.*, **495**, 134 (2001).
51. N. M. Markovic, H. A. Gasteiger, and P. N. Ross Jr., *J. Phys. Chem. Lett.*, **99**, 3411 (1995).
52. A. Lasia, in: B. E. Conway, J. O'M Bockris, and R. E. White, (Eds.), *Modern Aspects of Electrochemistry*, pp. 38, Kluwer/Plenum, New York, vol. 32, ch. 1 (1999).
53. B. Hirschorn, M. E. Orazem, B. Tribollet, V. Vivier, I. Frateurc, and M. Musianid, *Electrochim. Acta*, **55**, 6218 (2010).
54. A. S. Bondarenko, I. E. L. Stephens, H. A. Hansen, F. J. Perez-Alonso, V. Tripkovic, T. P. Johansson, J. Rossmeisl, J. K. Nørskov, and I. Chorkendorff, *Langmuir*, **27**, 2058 (2011).
55. P. M. Gomadam and J. W. Weidner, *Int. J. Energy Res.*, **29**, 1133 (2005).
56. M. Eikerling, A. A. Kornyshev, and E. Lust, *J. Electrochem. Soc.*, **152**, E24 (2005).
57. J.-B. Jorcin, M. E. Orazem, N. Pebere, and B. Tribollet, *Electrochim. Acta*, **51**, 1473 (2006).
58. M. H. Martin and A. Lasia, *Electrochim. Acta*, **54**, 5292 (2009).
59. T. Soboleva, Z. Xie, Z. Shi, E. Tsang, T. Navessin, and S. Holdcroft, *J. Electroanal. Chem.*, **622**, 145 (2008).
60. C. Gabrielli, P. P. Grand, A. Lasia, and H. Perrot, *J. Electrochem. Soc.*, **151**, A1943 (2004).
61. G. J. Brug, A. L. G. Van der Eeden, M. Sluyters-Rehbach, and J. H. Sluyters, *J. Electroanal. Chem.*, **176**, 275 (1984).
62. S. K. Roy, M. E. Orazem, and B. Tribollet, *J. Electrochem. Soc.*, **144**, B1378 (2007).
63. J. T. Muller, P. M. Urban, and W. F. Holderich, *J. Power Sources*, **84**, 157 (1999).
64. R. Makharia, M. F. Mathias, and D. R. Baker, *J. Electrochem. Soc.*, **152**, A970 (2005).
65. M. Mathias, D. Baker, J. Zhang, Y. Liu, and W. Gu, *ECS Trans.*, **13**, 129 (2008).
66. Z. B. -Saleh, A. Shahryari, and S. Omanovic, *Thin Solid Films*, **515**, 4727 (2007).
67. R. Kötz and M. Carlen, *Electrochim. Acta*, **45**, 2483 (2000).
68. D. Song, Q. Wang, Z. Liu, T. Navessin, M. Eikerling, and S. Holdcroft, *J. Power Sources*, **126**, 104 (2004).
69. C. Boyer, S. Gamburgzev, O. Velez, S. Srinivasan, and A. J. Appleby, *Electrochim. Acta*, **43**, 3703 (1998).
70. R. Rahul, R. K. Singh, and M. Neergat, *J. Electroanal. Chem.*, **712**, 223 (2014).
71. U. A. Paulus, A. Wokaun, G. G. Scherer, T. J. Schmidt, V. Stamenkovic, N. M. Markovic, and P. N. Ross, *Electrochim. Acta*, **47**, 3787 (2002).
72. R. Holze and W. Vielstich, *J. Electrochem. Soc.*, **131**, 2298 (1984).
73. M. Neergat and R. Rahul, *J. Electrochem. Soc.*, **159**, F234 (2012).
74. R. Devivaraprasad, R. Ramesh, N. Naresh, T. Kar, R. K. Singh, and M. Neergat, *Langmuir*, **30**, 8995 (2014).